Article:

Synthesis and dielectric characterisation of a low loss BaSrTiO₃/ABS ceramic/polymer composite for fused filament fabrication additive manufacturing

*Athanasios Goulas[1,2], Jack R. McGhee[2], Tom Whitaker[2], Daisy Ossai[2], Esha Mistry[2], Will Whittow[2], Bala Vaidhyanathan[1], Ian M. Reaney[3], John (Yiannis) C. Vardaxoglou[2], Daniel S. Engstrøm[2]

[1] Department of Materials, Loughborough University, Loughborough, LE11 3TU, United Kingdom.
[2] Wolfson School of Mechanical, Electrical and Manufacturing Engineering, Loughborough University, LE11 3TU, United Kingdom.
[3] Department of Materials Science and Engineering, University of Sheffield, Sheffield, S1 3JD, United Kingdom.

*a.goulas@lboro.ac.uk

ABSTRACT

Composite polymer/ceramic filaments for material extrusion-based fused filament fabrication additive manufacturing, using barium strontium titanium oxide (BST) ceramics and acrylonitrile butadiene styrene (ABS) thermoplastics were produced; their dielectric and physical properties have been characterised for the first time. The dielectric properties, relative permittivity (ε_r), quality factor ($Q{\times}f$) and dielectric loss ($tan\delta$) were measured as a function of ceramic solid loading (%) at 5 GHz for 3D printed samples. A relative permittivity ε_r = 6.05, $Q{\times}f$ =10,433 GHz and dielectric loss $tan\delta$ = 0.007 were obtained for a BST/ABS ceramic polymer composite, with 50 wt.% (15 vol.%) solid loading. The composite materials exhibit reduced dielectric losses compared to standard laminates currently used in the radiofrequency (RF) and telecommunications industry. Based on polymer/ceramic composite filament, a prototype microstrip patch 5G antenna and a hemispherical dielectric lens were designed and manufactured. Through testing, it shows good antenna performance with a centre frequency of f_0 = 3.78 GHz and a (−10 dB) bandwidth of 90.6 MHz. The dielectric lens increased the antenna gain by 3.86 dBi.

Keywords: additive manufacturing; 3D printing; fused filament fabrication; polymer ceramic composites; lens antennas

Graphical abstract
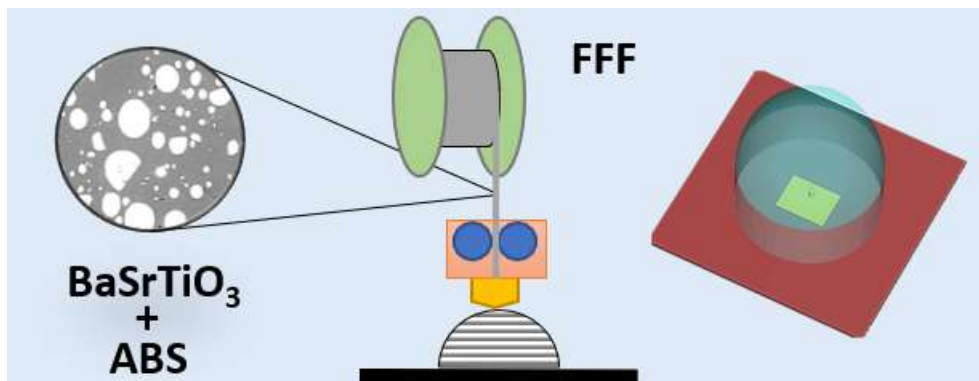
1. Introduction

There is an ongoing demand, for improved performance in electronic devices used in wireless radio communication equipment. Their performance relies on a combination of dielectric and physical properties, i.e., application-specific relative permittivity, low dielectric loss and high quality factor values ($Q{\times}f$ > 10,000 GHz), high thermal conductivity, low thermal expansion coefficient and high dimensional stability [1].

Ceramics have been the material of choice for the most part, as they exhibit low dielectric losses/high quality factors, they are dimensionally stable, they possess good mechanical properties and are available in a range of favourable relative permittivity values ε_r = 10 − 1000 [2–4]. However, ceramics are challenging to process and shape into components, especially when geometrically complex shapes are required, due their inherent high strength and brittle nature. Additionally, they often require complex synthesis routes and significant amounts of energy to be densified. Polymeric materials on the other hand, are easier to shape and form into components, but they lack the superior dielectric performance of their ceramic counterparts and are prone to distortions when operating at an extreme temperature environment, which limits their practical application. The relative permittivity of polymers are in the range of ε_r = 2 − 4 and the range for the dielectric losses is $tan\delta$ = 0.02 − 0.0001 [5,6].

Polymer/ceramic composite materials, that consist of a polymer matrix infilled with ceramic particles, have seen significant growth in the wireless radio communications industry. By combining the properties of both families of materials; namely the dielectric properties of the ceramics with the overall flexibility of polymers, key properties such as tailored relative permittivity, thermal expansion and low dielectric loss can be achieved.

Fused Filament Fabrication (FFF) is a material extrusion-based additive manufacturing process (ISO/ASTM 52903-1:2020), which uses thermoplastic filaments as feedstock [7]. FFF is a favourable 3D printing process for the rapid prototyping of novel design concepts in wireless radio telecommunications, given its affordable and easy-to-use nature [8–14]. However, the standard materials used in FFF (i.e. ABS, PLA, etc.) lack good dielectric properties such as low dielectric loss and higher relative permittivity values [15,16], which are necessary in order to realise more advanced device concepts such as 3D antennas, lenses etc. [17–19] and to achieve a high degree of miniaturisation; also offering volume and weight reduction.

Numerous studies on the formulation, dielectric and physical properties of polymer/ceramic materials for electronics applications are available in the literature [20–27]. However, they are predominantly focused on the dielectric properties of the bulk material composite and are not 3D printable.

Castles et al. reported the fabrication of a series of polymer/ceramic composite filaments for FFF, comprising of $BaTiO_3$ microparticle filler within an ABS polymer matrix. The microwave dielectric properties of 3D printed parts with $BaTiO_3$ solid loadings of up to 70 wt.%, were characterised at 15 GHz using a split post dielectric resonator, exhibited a highest relative permittivity value of ε_r = 8.72 ± 0.04 and dielectric losses of up to $tan\delta$ = 0.027 ± 0.012 [28]. In a follow-up paper from the same research group, Wu et al. presented the manufacture of an improved polymer/ceramic composite filament for FFF. The previous formulation was improved with the addition of a surfactant and plasticiser, to account for the volume fraction of the ceramic infilling particles. A filament with a maximum solid loading of 32 vol.% was manufactured; its dielectric properties measured at 15 GHz using a split post dielectric resonator were found to be ε_r = 11 ± 0.195 and $tan\delta$ = 0.0289 ± 0.12 [29]. Khatri et al. reported the fabrication of a series of composite filaments using the same combination of a $BaTiO_3$ microparticle ceramic filler and ABS as the polymer matrix. Composite filaments with a solid loading up to 35 vol.% were prepared and characterised, resulting into a mean relative permittivity of ε_r = 11.5 at 200 kHz [30].

To the best of the authors' knowledge, these three articles remain to-date, the only reported research on the synthesis of composite dielectric material filaments for FFF 3D printing.

This research article reports the synthesis of a novel ceramic particle-infilled composite material suitable for FFF 3D printing, comprising of a Barium Strontium Titanium Oxide filler and Acrylonitrile-Butadiene-Styrene matrix. The physical and dielectric properties at microwave frequencies of the as-discussed composite, were measured as a function of the amount of ceramic infilling material. Results from a 3D printable composite bearing the highest fraction of ceramic material thus high relative permittivity, were chosen to design, simulate and 3D print a patch antenna and a dielectric hemispherical lens as functional demonstrators. Results showcase the potential of this novel composite, when converted into a filament form, to be used for the rapid manufacture of functional prototypes or low volume fabrication of passive devices.

2. Materials and Methods

2.1. Materials

High-purity and commercially available barium strontium titanium oxide $BaSrTiO_3$ (BST) ceramic powder, in 77:23 wt.% ratio of Ba:Sr (99.8%, PI-KEM, Tamworth, Staffordshire, UK) was obtained, with an average particle size below 0.5 µm. Commercially available uncoloured pellets of Acrylonitrile Butadiene Styrene (ABS) thermoplastic were procured (ABS HI121H, LG Chem, Seoul, Korea) with a nominal density of 1.04 g/cm^3. BST was chosen as the infilling material, based on a combination of desirable dielectric properties; very high permittivity and low dielectric loss, at room temperature [31].

2.2. Composite filament manufacture

The ABS pellets were mixed together with Acetone in a 1:1.5 weight ratio and were left to dissolve over a period of 24 hours, while being continuously agitated with a magnetic stirrer. The resultant viscosity of the dissolved mixture allowed for the successful dispersion of the BST nanoparticles to form a slurry, without any visible sedimentation. Different weight fractions of BST ceramic powder were added to the dissolved ABS and were manually blended together by hand for 10 minutes. The obtained composites were poured into PTFE moulds and were left to dry in ambient air over a period of 48 hours. Once dried, the composites were pelletised, further dried in an oven at 80 °C for a period of 48 hours, then formed into 1.75 mm filaments using an extruder (Noztek Pro, Shoreham-by-Sea, Sussex, United Kingdom) at 220°C and 60 rpm.

2.3. Additive manufacturing

All manufacturing experiments were carried out on a multi-process additive manufacturing kit (Hydra 16A, Hyrel3D, Norcross, GA, USA) equipped with a filament extrusion module (MK1-250, Hyrel3D, Norcross, GA, USA), fitted with a brass nozzle of 0.55 mm diameter. All test samples were printed on top of a smooth borosilicate glass build surface, constantly heated at 100°C. A combination of extrusion temperature of 250°C, printing speed of 40 mm/s, layer thickness of 0.1 mm, 0.5 mm extrusion width; allowing for a 10 % overlap and a constant positive displacement value of 80 pulses per microlitre, were used to print rectangular test samples of 35 × 35 mm in size and 1 mm thickness. The test samples were first modelled using CAD and G-code for printing was generated using Hyrel3D's inbuilt slicing software.

2.4. Characterisation methods

The phase and purity of the purchased BST powder together with any potential interactions between the polymer matrix and the ceramic powder filler, were investigated using an X-Ray diffractometer (D2 Phaser, Bruker AXS, Karlsruhe, Germany) using CuK_α radiation at λ = 1.54054 Å, operating at 30 kV and 10 mA. 1 mm divergence and a 3 mm anti-scatter slits were used. Diffraction patterns were collected from 10 – 60° 2ϑ, using a 0.02° step size and 15/min sample rotation. Collected data were analysed using Bruker's proprietary software (DIFFRAC.EVA 5.2, Bruker AXS, Karlsruhe, Germany).

The apparent ($\rho_{measured}$) and relative density ($\rho_{relative}$) of the 3D printed test samples were measured following the Archimedes principle (ASTM D792-20), using an analytical balance (ME200, Mettler Toledo) using as reference the theoretical density ($\rho_{theoretical}$) of the composites. Results are reported as an average of five different 3D printed samples, together with their standard deviation.

The microstructures of the 3D printed test samples were analysed using a scanning electron microscope (SEM) (TM3030, Hitachi High Energy Technologies, etc.). 3D printed test samples were embedded in epoxy resin (EpoThin2, Buehler, Illinois, USA) and prepared for SEM by grinding using silicon carbide paper of P1200 grit size, followed by polishing on a cloth impregnated with a 0.05 μm alumina suspension. To prevent charging during SEM, samples were sputter coated with a gold/palladium alloy in an 80:20 wt.% ratio, for 90 s at 25 mA (Quorum Q150T, Quorum, Edwards, Hastings, UK).

Relative permittivity (ε_r), dielectric loss ($tan\delta$) and quality factor ($Q \times f$) of additively manufactured BST/ABS samples were determined by placing the rectangular 3D printed test samples of 35 × 35 mm and 1 mm thickness, into a split post dielectric resonator (SPDR) operating at 5 GHz (QWED, Warsaw, Poland). The properties were calculated using QWED's proprietary software. Results are reported as an average of five different 3D printed samples, together with standard deviation.

A fully anechoic chamber (NSI-MI Technologies, Suwanee, GA, USA) was used to measure the performance of the prototype patch antenna and hemispherical dielectric lens manufactured in this study.

3. Results and Discussion

3.1. Raw materials characterisation

Figure 1a, shows the X-ray diffraction patterns of as-purchased BST powder used in this study. The diffraction peaks from the BST powder were indexed to the tetragonal $Ba_{0.77}Sr_{0.23}TiO_3$ phase of the *P4mm* group, with lattice parameters $a = b = 3.977710$ Å and $c = 3.98830$ Å (ICDD PDF 44-0093). A small diffraction peak at $2\vartheta = 24.02°$ was indexed to $BaCO_3$ (PDF 05-0378), which is used as a precursor for the solid-state synthesis of BST. The theoretical density of the identified BST phase was calculated from the XRD measured data at $\rho_{BST} = 5.838$ g/cm^3. **Figure 1b,** shows the BST particles which are submicron in diameter.
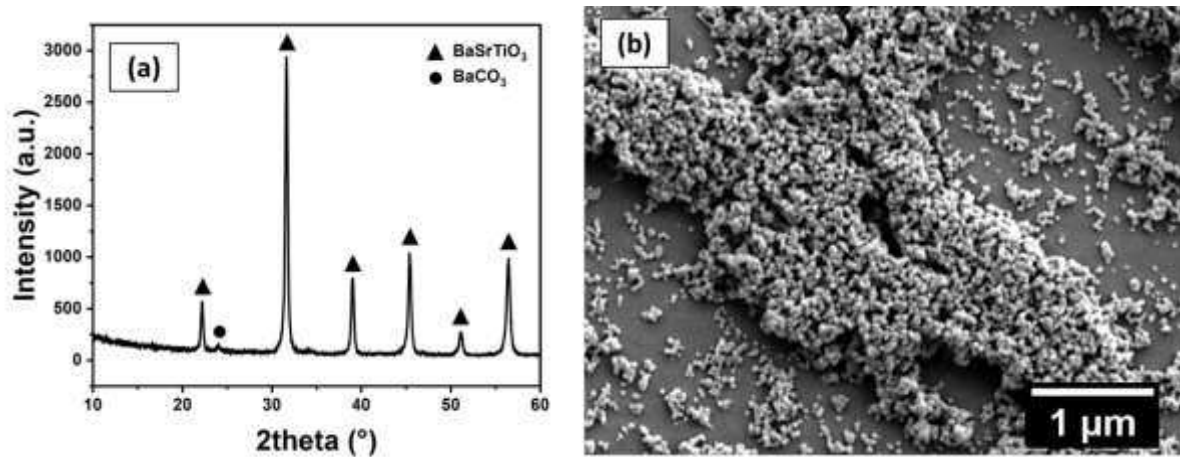

Figure 1 – (a) X-Ray diffraction patterns, (b) SEM of the Barium Strontium Titanate powder.

3.2. Physical and dielectric properties of the 3D printed test samples

The microwave dielectric properties (relative permittivity, dielectric loss and quality factor) measured at 5 GHz of the polymer/ceramic 3D printed test samples, are shown in **Figure 2**, as a function of the ceramic particle solid loading (wt.%). A progressive increase in ε_r from 2.66 ± 0.03 (unfilled ABS 3D printed sample, 0 wt.%) to 6.05 ± 0.36 for the BST/ABS composite with 50.27 wt.% (15.26 vol.%) was observed, due to the higher dielectric constant of the infilling ceramic particles. However, this was accompanied by a reduction in $Q \times f$ and tanδ from 28,107 ± 601 GHz and 0.005 ± 0.0001 to 10,433 ± 442 GHz and 0.007 ± 0.0002 for 0 and 50.27 wt.%, respectively. There are several mechanisms which contribute to the increase in *tanδ,* including i) an increase in its average value for the composite as the BST (*tanδ* ≈ 0.01) concentration increases and ii) the formation of polymer/ceramic interfaces throughout the sample which are a source of anharmonicity in the vibrational phonon modes that

contribute to the dielectric loss at microwave frequencies. Anharmonicity is generally associated with an increase in imperfections in the polymer matrix and/or crystal lattice of the ceramic fillers, the disorder between the matrix/filler interphase region and finally iii) impurities within the polymer matrix [1]. The composites manufactured in this study, exhibit consistent dielectric properties ($\sigma \leq 6\%$) and lower losses than laminate-based substrates such as FR-4 (ε_r = 4.98 ± 0.001, $Q{\times}f$ = 973 ± 6 GHz and $tan\delta$ = 0.014 ± 0.0001, at 5 GHz as measured in the lab) that are commonly used in the telecommunications industry or for prototyping.
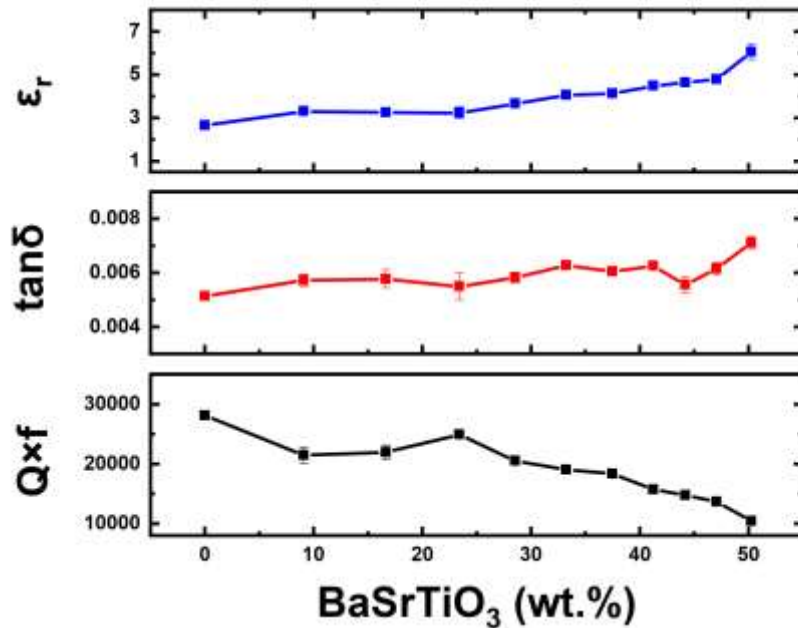

Figure 2 – BST/ABS Mass Fraction vs. Relative Permittivity (ε_r), Dielectric Loss ($tan\delta$) and Quality Factor ($Q{\times}f$) of the 3D printed test samples, measured at 5 GHz using the SPDR.

Figure 3a, shows the apparent ($\rho_{measured}$), relative ($\rho_{relative}$) and theoretical ($\rho_{theoretical}$) densities of the BST/ABS ceramic composites. The apparent density of the composites increased with increasing ceramic solid loading, due to the higher density of the infilling ceramic material. However, the relative density was decreased as a function of the ceramic solid loading, due increased porosity in the 3D printed samples. Porosity in the 3D printed samples is due to factors, such as the poor adhesion between the ceramic particles and the polymer matrix [32] and the reduction of the expansion coefficient of the composite material [33], causing the prints to be prone to defects such as interlaminar porosity. **Figure 4**, depicts the microstructure of a 3D printed polymer/ceramic sample bearing a 50.27 wt.% BST loading. The bright regions are clusters formed by the agglomerated BST ceramic particles, whereas the darker regions are the ABS matrix. The areas shown with arrows, highlight the poor ceramic-to-polymer adhesion and interlaminar porosity defects discussed in this section. Particle agglomerates; a result of electrostatic attraction, are a common occurrence with submicron solid particles being dispersed into heterogenous media. Unless treated with a dispersing

agent prior to mixing, they are very likely to cause the deterioration of the materials' properties at larger particle loadings. However, given their very low concentration (15.26 vol.%) and relatively small size at less than 100 μm in diameter, their influence is considered negligible in terms of anisotropy, as previously found and discussed in [28]. For the above-mentioned reasons, filaments with a solid loading above 50.25 wt.% (15.26 vol.%) exhibited a brittle nature and poor extrudability; no further manufacture or characterisation thereof was pursued. No additives, such as a dispersant or a plasticiser were used for the synthesis of this polymer ceramic composite, as their use was expected to contribute to dielectric losses.
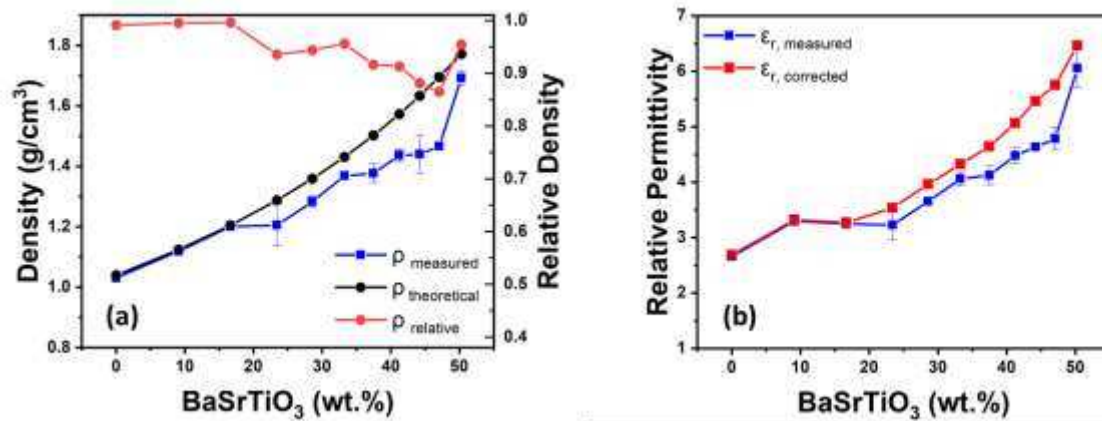

Figure 3 – BST/ABS solid loading vs. (a) Density of 3D Printed test samples, (b) measured and corrected for porosity relative permittivity values of the 3D printed test samples at 5 GHz.

Porosity is a common processing defect for FFF 3D printed parts [8] due to a number of reasons, such as unoptimized choice of 3D printing process parameters, or the inherent flow properties of the materials during extrusion [34]. Both led to a collective increase in porosity, which in turn resulted in the deterioration of the dielectric and associated physical properties of the composite. Therefore, to eliminate the influence of pores on the bulk permittivity of the printed ceramic composite, the following equation [35] was used:

$$\varepsilon_r = \varepsilon_{measured} \times 1 + (1.5 \times Porosity) \qquad \text{Equation (1)}$$

It should be noted that the composite could be successfully deposited over a wide range of printing parameters (i.e., printing speed, extrusion temperature etc.), however no optimisation of the printing properties was sought as this was not the objective of this study. The printing parameters used in this study have been chosen based on empirical knowledge.

Figure 3b, shows an overlay of the measured relative permittivity values ($\varepsilon_{measured}$) against the corrected-for-porosity relative permittivity values ($\varepsilon_{corrected}$), of the 3D printed test specimens, as a function of solid loading. Porosity was calculated as the difference between the theoretical ($\rho_{theoretical}$) and measured ($\rho_{measured}$) densities. **Table 1,** contains a list of all the dielectric and physical properties of the 3D printed test samples fabricated in this study.

Table 1 - Dielectric and physical properties of 3D printed BST/ABS composites, with standard deviation (n=5).

| BST/ABS wt.%	BST/ABS (vol.%)	$\varepsilon_r \pm \sigma$	$tan\delta \pm \sigma$	$Q \times f \pm \sigma$ (GHz)	$\rho \pm \sigma$ (g/cm³)	ρ_{theor} (g/cm³)	$\rho_{relative}$ (g/cm³)	$\varepsilon_{r\ corrected}$
0	0	2.66 ± 0.03	0.005 ± 0.0001	28,107 ± 601	1.03 ± 0.01	1.04	0.991	2.69
9.10	1.75	3.30 ± 0.08	0.006 ± 0.0002	21,439 ± 1371	1.12 ± 0.01	1.12	0.995	3.32
16.64	3.43	3.25 ± 0.09	0.006 ± 0.0003	21,941 ± 1232	1.20 ± 0.01	1.20	0.996	3.27
23.40	5.16	3.23 ± 0.27	0.005 ± 0.0005	24,888 ± 607	1.20 ± 0.07	1.29	0.935	3.54
28.56	6.65	3.65 ± 0.08	0.006 ± 0.0002	20,503 ± 659	1.28 ± 0.02	1.36	0.944	3.96
33.25	8.15	4.06 ± 0.12	0.006 ± 0.0001	19,042 ± 465	1.37 ± 0.00	1.43	0.956	4.32
37.46	9.64	4.12 ± 0.17	0.006 ± 0.0001	18,383 ± 520	1.38 ± 0.03	1.50	0.91	4.64
41.24	11.11	4.48 ± 0.15	0.006 ± 0.0002	15,721 ± 709	1.44 ± 0.02	1.57	0.912	5.06
44.20	12.37	4.64 ± 0.04	0.006 ± 0.0003	18,920 ± 1399	1.30 ± 0.04	1.63	0.881	5.46
47.05	13.67	4.78 ± 0.21	0.006 ± 0.0002	13,662 ± 750	1.47 ± 0.03	1.70	0.864	5.75
50.27	15.26	6.05 ± 0.36	0.007 ± 0.0002	10,433 ± 442	1.69 ± 0.02	1.77	0.955	6.46
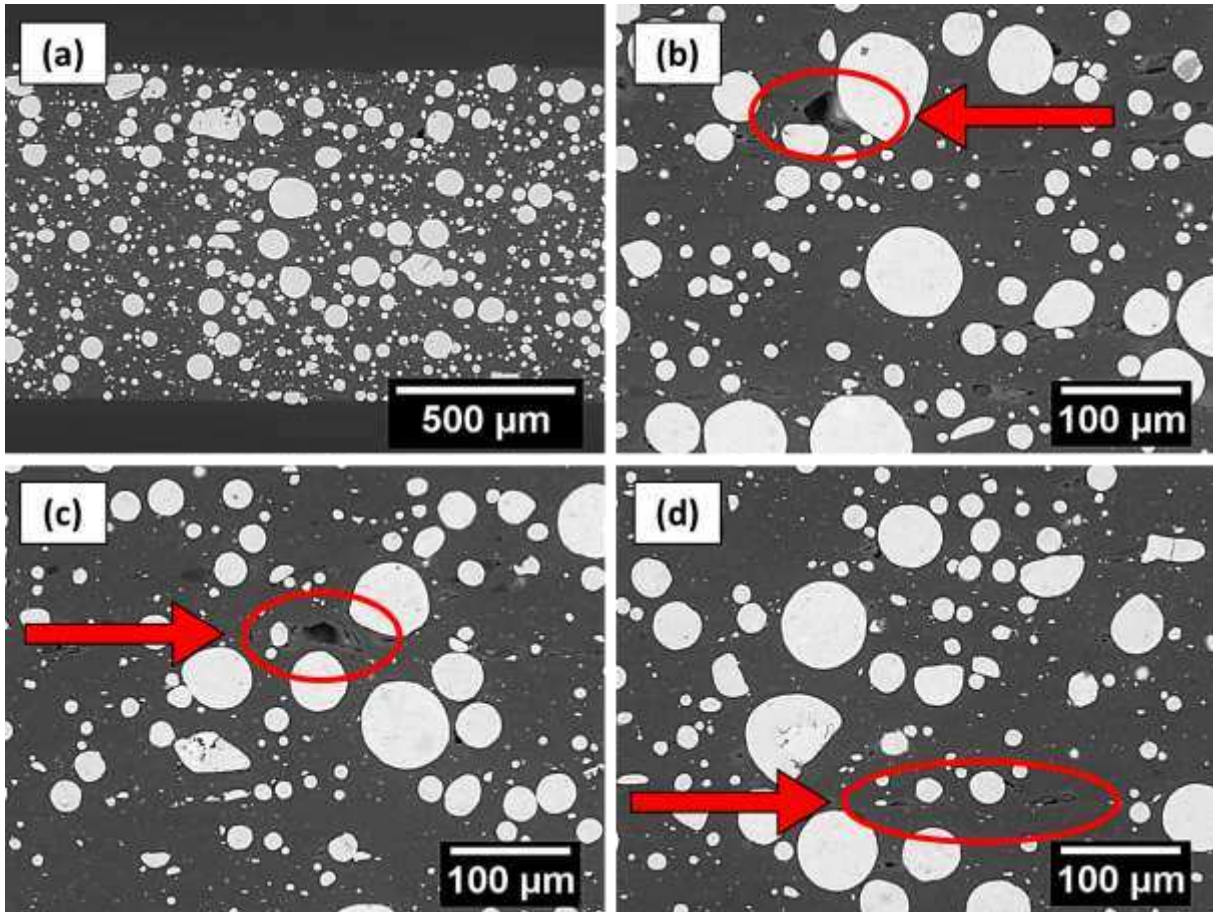
Figure 4 – (a-d) SEM of cross-sectioned BST/ABS 3D printed test samples at 50.27 wt.% (15.26 vol.%). The arrows denote the defects responsible for hampering the dielectric and physical properties.
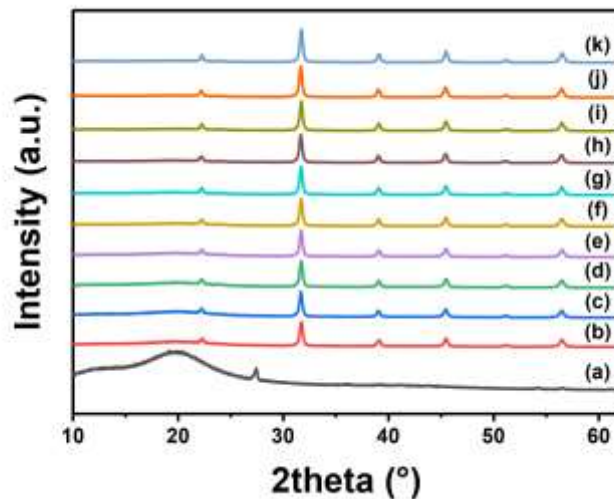
3.3. X-Ray Diffraction

Figure 5 – Diffraction pattern overlay of 3D printed BST/ABS composites. (a = 0 wt.%, b = 9.10 wt.%. c = 16.64 wt.%, d = 23.40 wt.%, e = 28.56 wt.%, f = 33.25 wt.%, g = 37.46 wt.%, h = 41.24 wt.%, I = 44.20 wt.%, j = 47.05 wt.% and k = 50.27 wt.%)

Figure 5(a-k) shows the X-ray diffraction patterns of the BST/ABS composites with 0 – 50.27 wt.% BST ceramic solid loading. The diffraction pattern **Figure 5a** from the unloaded polymer showed a characteristic amorphous halo at low 2ϑ angles, followed by a low intensity diffraction peak at 2ϑ = 27°, which is typical for the weekly crystalline ABS [36]. For the polymer/ceramic mixtures shown in **Figure 5b-k**, the diffraction peaks in the composites are indexed according to the $Ba_{0.77}Sr_{0.23}TiO_3$ phase, as discussed in (**Section 3.1**). As the concentration of the ceramic filler increases, the diffraction intensity of the ABS disappeared into the background of the XRD spectra. The results indicate that BST and ABS remain as a heterogenous mixture regardless of the solid loading of the ceramic particles.

3.4. Manufacture and measurements of a prototype patch antenna and a hemispherical dielectric lens

Microstrip patch antennas are a popular choice in modern RF electronics due their ease of fabrication and small form factor for integration within limited space [37]. A patch antenna consists of a radiating patch element and a ground plane which are separated by a dielectric substrate. The properties of the dielectric substrate are important as they influence the resonant frequency and antenna gain; Increasing the ε_r of the substrate can be used to miniaturise the design [38] but may also affect the antenna's bandwidth and overall efficiency [39].

A rectangular microstrip patch antenna (**Figure 6**) operating in a middle frequency band (2.3 – 4.7 GHz) of the 5G spectrum, was first simulated in Microwave CST Studio using the dielectric properties of the 50.27 wt.% (15.26 vol.%) composite; shown in **Table 1**, and was then fabricated using a $35 \times 35 \times 1$ mm^3 substrate, via FFF 3D printing. The radiation element and ground plane were painted on with a silver conductive paint (RS Pro silver conductive paint, ≈ 200 µm thick) which had a datasheet resistivity of 0.001 Ω·cm. The radiating patch element had dimensions of 20.5×15.3 mm and the ground plane completely covered the reverse side of the dielectric substrate. A coaxial probe feed was used, 2.9 mm from the long edge of the radiation element. These dimensions resulted in a well matched microstrip patch antenna, operating at a resonant frequency of 3.78 GHz with an S11 null of -21.25 dB and a -10 dB bandwidth of 90.6 MHz. Measurements of the antenna gain and total efficiency, are within reasonable agreement with simulation data (less than 0.5 dBi difference for the antenna gain and less than 5% difference for the total efficiency). The antenna performance confirms the potential of the BST/ABS composites to be used for prototyping antenna structures, where using materials with higher permittivity values, can enable miniaturisation.
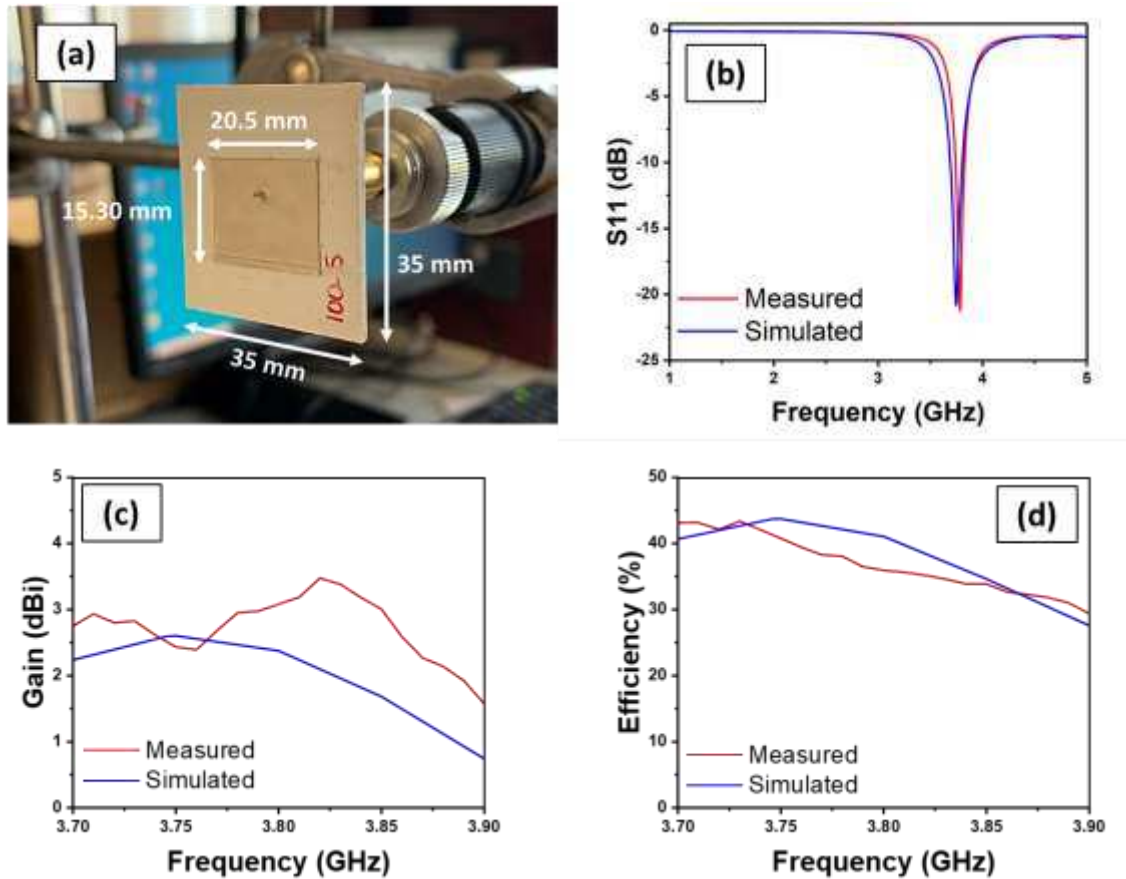
Figure 6 – (a) Probe-fed microstrip patch antenna operating at a 3.78 GHz, using a 3D printed BST/ABS composite substrate, measured vs. simulated results (b) reflection coefficient, (c) gain and (d) total efficiency.

Dielectric lenses are passive antenna components used for improving antenna gain and other radiation characteristics (directivity, beam forming etc). Despite their easy-to-shape form, costs for conventional manufacture remain significant, where 3D printing could offer a significant reduction towards the manufacturing-related costs. A hemispherical dielectric lens of 25 mm radius fed with a different microstrip patch antenna operating at 9.95 GHz, was first simulated in Microwave CST Studio, using the dielectric properties of the 50.27 wt.% (15.26 vol.%) BST/ABS composite and was then fabricated using FFF 3D printing using a 100 % infill setting. The hemispherical lens (shown in **Figure 7**) was positioned on top of the patch antenna, using a D20 × 8 mm 3D printed spacer, using cyclic olefin copolymer (COC); an ultra-low-loss and low permittivity thermoplastic material for FFF (*tanδ* ≈ 0.0001 at 5 GHz) using a 10 % infilling factor. This spacer was printed with a very low infill percentage to exhibit dielectric properties close to that of free space and hence does not affect the resonant frequency of the patch antenna underneath. The patch antenna was manufactured from a sheet of 0.51 mm thick, Rogers 4350B, copper clad commercial laminate. The radiating element was then fed from behind with a coaxial probe feed.
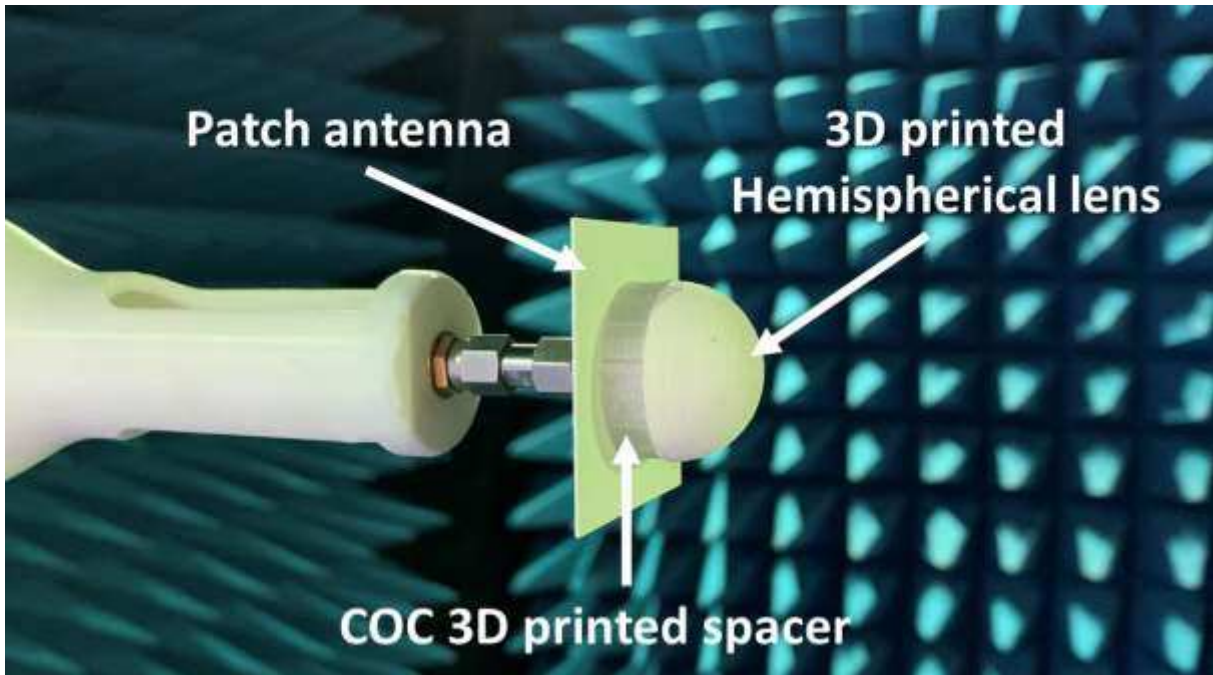
Figure 7 - 3D printed hemispherical dielectric lens using a BST/ABS composite.

Figure 8, contains the antenna gain, directivity and total efficiency plots of the microstrip antenna, where **Figure 9** shows the radiation patterns, with and without the hemispherical dielectric lens, as measured inside a fully anechoic chamber. The antenna without the lens, had a maximum gain of 4.92 dBi, a directivity of 6.84 dBi and a total efficiency of 65.8 % at 9.85 GHz. The addition of the 3D printed BST/ABS hemispherical lens caused an increase in both gain and directivity at 8.78 dBi and 10.66 dBi accordingly. There was a minimal decrease in the total efficiency to 64.8 %, however this is within the measurement accuracy of the anechoic chamber used and thus the losses due to the lens can be considered negligible.
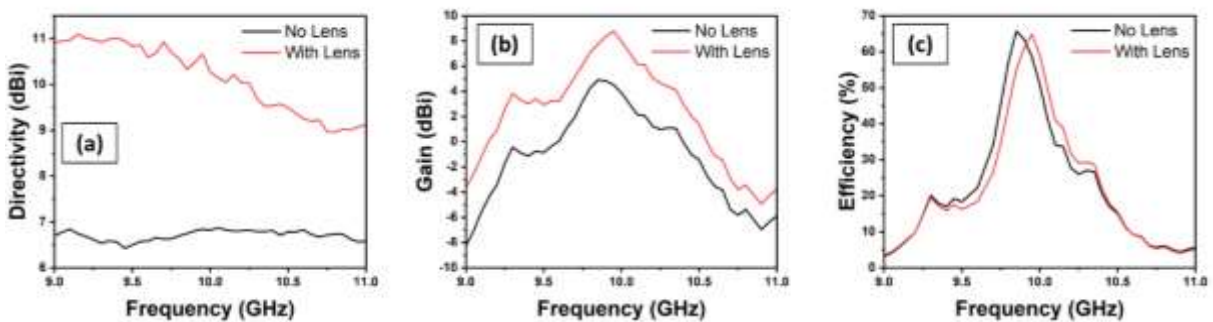

Figure 8 – Measured antenna results (a) Antenna Directivity, (b) Antenna Gain and (c) Total Efficiency of the antenna with/without the 3D printed hemispherical lens.
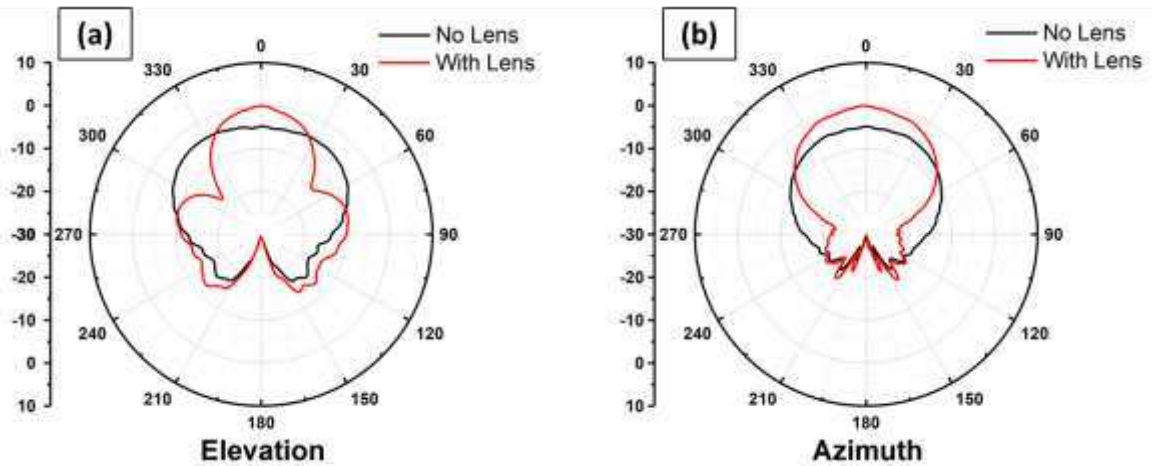
Figure 9 – Measured radiation patterns in (a) Elevation and (b) Azimuth planes of the hemispherical dielectric lens above the patch antenna

4. Conclusions

This experimental study investigated the synthesis and dielectric characterisation of a novel polymer ceramic composite as a feedstock filament for FFF 3D printing. The results show that a novel low-loss polymer/ceramic composite with desirable and bespoke ε_r has been fabricated.

- Composite polymer/ceramic filament of 1.75 mm in diameter, comprising of submicron BaSrTiO$_3$ fillers within an ABS thermoplastic polymer matrix were synthesised for FFF.
- A maximum obtained solid loading of 50.27 wt.% (15.26 vol.%) ceramic particles, resulted in a low loss composite with ε_r = 6.05 ± 0.36, *tanδ* = 0.007 ± 0.0002 and $Q{\times}f$ = 10,433 ± 442 GHz at 5 GHz with having ρ_{rel}= 95.5%.
- The composite with the maximum ceramic infill, corrected for porosity had ε_r = 6.46.
- A prototype microstrip patch antenna was fabricated, by exploiting the dielectric properties of the BST/ABS composite. Good agreement of measured vs. simulated values of the reflection loss parameters (S11), antenna gain and total efficiency, were obtained at the resonant frequency of f_0 = 3.78 GHz.
- A prototype hemispherical dielectric lens was also fabricated by FFF using the BST/ABS composite. The lens increased the gain by 3.86 dB, with negligible effect on the antenna efficiency.

Declaration of competing interests

The authors declare that they have no known competing financial interests or personal relationships that could have appeared to influence the work reported in this paper.

CRediT

Athanasios Goulas: Conceptualization, methodology, investigation, visualization, writing - original draft. **Jack R. McGhee:** Investigation, writing - review and editing. **Daisy Ossai & Esha Mistry:** Investigation. **Tom Whittaker:** Investigation, writing - review and editing. **Bala Vaidhyanathan** and **Ian M. Reaney:** Supervision, writing - review and editing. **Will Whittow:** Supervision, writing - review and editing. **John (Yiannis) C. Vardaxoglou:** Supervision, writing - review and editing. **Daniel S. Engstrøm:** Supervision, writing - review and editing.

Data availability

The raw/processed data required to reproduce these findings cannot be shared at this time as the data also forms part of an ongoing study.

References

[1] R. Ratheesh, M.T. Sebastian, Polymer-Ceramic Composites for Microwave Applications, in: Microw. Mater. Appl. 2V Set, 2017: pp. 481–535. https://doi.org/10.1002/9781119208549.ch11.

[2] A. Goulas, G. Chi-Tangyie, D. Wang, S. Zhang, A. Ketharam, B. Vaidhyanathan, I.M. Reaney, D.A. Cadman, W.G. Whittow, J. (Yiannis) C. Vardaxoglou, D.S. Engstrøm, Additively manufactured ultra-low sintering temperature, low loss Ag2Mo2O7 ceramic substrates, J. Eur. Ceram. Soc. 41 (2020) 394–401. https://doi.org/10.1016/j.jeurceramsoc.2020.08.031.

[3] T. Tsurumi, T. Sekine, H. Kakemoto, T. Hoshina, S.M. Nam, H. Yasuno, S. Wada, Evaluation and statistical analysis of dielectric permittivity of BaTiO3 powders, J. Am. Ceram. Soc. 89 (2006) 1337–1341. https://doi.org/10.1111/j.1551-2916.2005.00905.x.

[4] I.M. Reaney, D. Iddles, Microwave dielectric ceramics for resonators and filters in mobile phone networks, J. Am. Ceram. Soc. 89 (2006) 2063–2072. https://doi.org/10.1111/j.1551-2916.2006.01025.X.

[5] T. Zhou, J.-K. Yuan, S.-T. Li, G.-H. Hu, J.-W. Zha, Z.-M. Dang, Fundamentals, processes and applications of high-permittivity polymer–matrix composites, Prog. Mater. Sci. 57 (2011) 660–723. https://doi.org/10.1016/j.pmatsci.2011.08.001.

[6] J. Varghese, N. Joseph, H. Jantunen, S.K. Behera, H.T. Kim, M.T. Sebastian, Microwave Materials for Defense and Aerospace Applications, 2019. https://doi.org/10.1007/978-3-319-73255-8_9-1.

[7] ISO / ASTM52903-1:2020(E), Additive manufacturing — Material extrusion-based additive manufacturing of plastic materials — Part 1: Feedstock materials, ASTM Int. West Conshohocken, PA. 2020 (2017) 1–20.

[8] A. Goulas, S. Zhang, J.R. Mcghee, D.A. Cadman, W.G. Whittow, J.C.V. Yiannis, D.S. Engstrøm, Fused filament fabrication of functionally graded polymer composites with variable relative permittivity for microwave devices, Mater. Des. 193 (2020) 108871. https://doi.org/10.1016/j.matdes.2020.108871.

[9] O. Kaynan, A. Yıldız, Y.E. Bozkurt, E. Ozden Yenigun, H. Cebeci, Electrically conductive high-performance thermoplastic filaments for fused filament fabrication, Compos. Struct. 237 (2020). https://doi.org/10.1016/j.compstruct.2020.111930.

[10] P. Parsons, Z. Larimore, F. Muhammed, M. Mirotznik, Fabrication of low dielectric constant composite filaments for use in fused filament fabrication 3D printing, Addit. Manuf. 30 (2019) 100888. https://doi.org/10.1016/j.addma.2019.100888.

[11] P. Parsons, Z. Larimore, M. Mirotznik, G. Mitchell, Composite materials development for fused filament fabrication of RF systems, Appl. Comput. Electromagn. Soc. J. 35 (2020) 1278–1279. https://doi.org/10.47037/2020.ACES.J.351108.

[12] T. Tichy, O. Sefl, P. Vesely, T. Capal, Application Possibilities of Fused Filament Fabrication Technology for High-Voltage and Medium-Voltage Insulation Systems, Proc. Int. Spring Semin. Electron. Technol. 2019-May (2019) 1–6. https://doi.org/10.1109/ISSE.2019.8810300.

[13] M. Mirzaee, S. Noghanian, L. Wiest, I. Chang, Developing flexible 3D printed antenna using conductive ABS materials, IEEE Antennas Propag. Soc. AP-S Int. Symp. 2015-Octob (2015) 1308–1309. https://doi.org/10.1109/APS.2015.7305043.

[14]	M. Mirzaee, S. Noghanian, High frequency characterisation of wood-fill PLA for antenna additive manufacturing application, Electron. Lett. 52 (2016) 1656–1658. https://doi.org/10.1049/el.2016.2505.

[15]	C. Lee, J. McGhee, C. Tsipogiannis, S. Zhang, D. Cadman, A. Goulas, T. Whittaker, R. Gheisari, D. Engstrom, J. (Yiannis) Vardaxoglou, W. Whittow, Evaluation of Microwave Characterization Methods for Additively Manufactured Materials, Designs. 3 (2019). https://doi.org/10.3390/designs3040047.

[16]	J. Sun, A. Dawood, W.J. Otter, N.M. Ridler, S. Lucyszyn, Microwave Characterization of Low-Loss FDM 3-D Printed ABS with Dielectric-Filled Metal-Pipe Rectangular Waveguide Spectroscopy, IEEE Access. 7 (2019) 95455–95486. https://doi.org/10.1109/ACCESS.2019.2926717.

[17]	S. Zhang, Three-dimensional printed millimetre wave dielectric resonator reflectarray, IET Microwaves, Antennas Propag. 11 (2017) 2005–2009. https://doi.org/10.1049/iet-map.2017.0278.

[18]	J.M. Monkevich, G.P. Le Sage, Design and Fabrication of a Custom-Dielectric Fresnel Multi-Zone Plate Lens Antenna Using Additive Manufacturing Techniques, IEEE Access. 7 (2019) 61452–61460. https://doi.org/10.1109/ACCESS.2019.2916077.

[19]	J. Huang, S.J. Chen, Z. Xue, W. Withayachumnankul, C. Fumeaux, Wideband endfire 3-d-printed dielectric antenna with designable permittivity, IEEE Antennas Wirel. Propag. Lett. 17 (2018) 2085–2089. https://doi.org/10.1109/LAWP.2018.2857497.

[20]	C.K. Chiang, R. Popielarz, Polymer Composites with High Dielectric Constant, Ferroelectrics. 275 (2010) 1–9. https://doi.org/10.1080/00150190190021786.

[21]	G. Subodh, V. Deepu, P. Mohanan, M.T. Sebastian, Polystyrene/Sr2Ce2Ti5O15 composites with low dielectric loss for microwave substrate applications, Polym. Eng. Sci. 49 (2009) 1218–1224. https://doi.org/10.1002/pen.21220.

[22]	F.A. Pearsall, I. Kymissis, P. Kinget, S.R. Sanders, D. Steingart, S. O'Brien, J. Lombardi, N. Farahmand, B. Van Tassel, E.S. Leland, L. Huang, S. Liu, S. Yang, C. Le, Polymer-Nanocrystal Nanocomposites: Device Concepts in Capacitors and Multiferroics, IEEE Trans. Nanotechnol. 19 (2020) 255–268. https://doi.org/10.1109/TNANO.2019.2939093.

[23]	T. Hanemann, D.V. Szabó, Polymer-nanoparticle composites: From synthesis to modern applications, 2010. https://doi.org/10.3390/ma3063468.

[24]	L. Yao, Z. Pan, J. Zhai, G. Zhang, Z. Liu, Y. Liu, High-energy-density with polymer nanocomposites containing of SrTiO3 nanofibers for capacitor application, Compos. Part A Appl. Sci. Manuf. 109 (2018) 48–54. https://doi.org/10.1016/j.compositesa.2018.02.040.

[25]	S. Koulouridis, G. Kiziltas, Y. Zhou, D.J. Hansford, J.L. Volakis, Polymer-ceramic composites for microwave applications: Fabrication and performance assessment, IEEE Trans. Microw. Theory Tech. 54 (2006) 4202–4208. https://doi.org/10.1109/TMTT.2006.885887.

[26]	S.L. Liu, J. Bian, Low dielectric loss LNT/PEEK composites with high mechanical strength and dielectric thermal stability, Int. J. Appl. Ceram. Technol. 17 (2020) 1341–1347. https://doi.org/10.1111/ijac.13378.

[27]	S.W. Kwok, K.H.H. Goh, Z.D. Tan, S.T.M. Tan, W.W. Tjiu, J.Y. Soh, Z.J.G. Ng, Y.Z. Chan, H.K. Hui, K.E.J. Goh, Electrically conductive filament for 3D-printed circuits and sensors, Appl. Mater. Today. 9 (2017) 167–175. https://doi.org/10.1016/j.apmt.2017.07.001.

[28] F. Castles, D. Isakov, A. Lui, Q. Lei, C.E.J. Dancer, Y. Wang, J.M. Janurudin, S.C. Speller, C.R.M. Grovenor, P.S. Grant, Microwave dielectric characterisation of 3D-printed BaTiO3/ABS polymer composites, Sci. Rep. 6 (2016) 1–8. https://doi.org/10.1038/srep22714.

[29] Y. Wu, D. Isakov, P.S. Grant, Fabrication of composite filaments with high dielectric permittivity for fused deposition 3D printing, Materials (Basel). 10 (2017). https://doi.org/10.3390/ma10101218.

[30] B. Khatri, K. Lappe, M. Habedank, T. Mueller, C. Megnin, T. Hanemann, Fused deposition modeling of ABS-barium titanate composites: A simple route towards tailored dielectric devices, Polymers (Basel). 10 (2018). https://doi.org/10.3390/polym10060666.

[31] B.A. Baumert, L.H. Chang, A.T. Matsuda, T.L. Tsai, C.J. Tracy, R.B. Gregory, P.L. Fejes, N.G. Cave, W. Chen, D.J. Taylor, T. Otsuki, E. Fujii, S. Hayashi, K. Suu, Characterization of sputtered barium strontium titanate and strontium titanate-thin films, J. Appl. Phys. 82 (1997) 2558–2566. https://doi.org/10.1063/1.366066.

[32] S. George, M.T. Sebastian, Enhanced Permittivity by the Adhesion of Conducting and Low-Loss Insulating Ceramics in Polystyrene, J. Appl. Polym. Sci. 114 (2009) 1682–1686. https://doi.org/10.1002/app.

[33] S. Thomas, V. Deepu, S. Uma, P. Mohanan, J. Philip, M.T. Sebastian, Preparation, characterization and properties of Sm2Si2O7 loaded polymer composites for microelectronic applications, Mater. Sci. Eng. B Solid-State Mater. Adv. Technol. 163 (2009) 67–75. https://doi.org/10.1016/j.mseb.2009.05.007.

[34] A. Goulas, S. Zhang, D.A. Cadman, J. Järveläinen, V. Mylläri, W.G. Whittow, J.Y.C. Vardaxoglou, D.S. Engstrøm, The Impact of 3D Printing Process Parameters on the Dielectric Properties of High Permittivity Composites, Designs. 3 (2019). https://doi.org/https://doi.org/10.3390/designs3040050.

[35] D. Zhou, H. Wang, X. Yao, L.-X. Pang, Microwave Dielectric Properties of Low Temperature Firing $Bi_2Mo_2O_9$ Ceramic, J. Am. Ceram. Soc. 91 (2008) 3419–3422. https://doi.org/10.1111/j.1551-2916.2008.02596.x.

[36] M.I. Mohammed, D. Wilson, E. Gomez-Kervin, B. Tang, J. Wang, Investigation of Closed-Loop Manufacturing with Acrylonitrile Butadiene Styrene over Multiple Generations Using Additive Manufacturing, ACS Sustain. Chem. Eng. 7 (2019) 13955–13969. https://doi.org/10.1021/acssuschemeng.9b02368.

[37] D. Wang, B. Siame, S. Zhang, G. Wang, X. Ju, J. Li, Z. Lu, Y. Vardaxoglou, W. Whittow, D. Cadman, S. Sun, D. Zhou, K. Song, I.M. Reaney, Direct Integration of Cold Sintered, Temperature-Stable Bi2Mo2O9-K2MoO4 Ceramics on Printed Circuit Boards for Satellite Navigation Antennas, J. Eur. Ceram. Soc. (2020) 0–1. https://doi.org/10.1016/j.jeurceramsoc.2020.04.025.

[38] L. Zhang, J. Zhang, Z. Yue, L. Li, Thermally stable polymer–ceramic composites for microwave antenna applications, J. Adv. Ceram. 5 (2016) 269–276. https://doi.org/10.1007/s40145-016-0199-8.

[39] D. Wang, S. Zhang, G. Wang, Y. Vardaxoglou, W. Whittow, D. Cadman, D. Zhou, K. Song, I.M. Reaney, Cold sintered CaTiO3-K2MoO4 microwave dielectric ceramics for integrated microstrip patch antennas, Appl. Mater. Today. 18 (2020) 100519. https://doi.org/10.1016/j.apmt.2019.100519.